

Uncertainty Analysis
for the KCS Model
(SRI M.S. No. 631) Tests
in the SRI 400m Towing Tank

Report of
Ship Performance Division

SHIP PERFORMANCE DIVISION
SHIP RESEARCH INSTITUTE
MINISTRY OF TRANSPORT
6-38-1, SHINKAWA
MITAKA, TOKYO 181, JAPAN

Ship Performance Division
The Ship Research Institute
The Ministry of Transport

Unclassified

SPD Report
No. 00-008-1

Uncertainty Analysis
for the KCS Model
(SRI M.S. No. 631) Tests
in the SRI 400m Towing Tank

Kenichi KUME, Yoshitaka UKON, Junichi FUJISAWA,
Toshifumi HORI, Toshiaki TSUKADA, Haruya TAKESHI

June 1, 2000

Research on Systematic Experiments for Evaluating Ship Performance in Seaway

Project Manager



Chief of Section



Director



Uncertainty Analysis for the KCS Model (SRI M.S.No.631) Test in the SRI 400m Towing Tank

1. Introduction

Recently, demands for reporting experimental uncertainties for the measurements in towing tank experiments have increased more than ever. The 22nd ITTC Resistance Committee recommended that AIAA uncertainty assessment methodology should be adopted as the ITTC standard for towing tank experiments [1]. At the Ship Research Institute (SRI), efforts have been made on the uncertainty analysis for towing tank experiments over the past several years [2,3].

The present report describes the uncertainty analysis for the surface pressure and local velocity field measurements around a ship model of a 3,600TEU Korea Research Institute of Ships and Ocean Engineering (KRISO) container ship (KCS) for the International Workshop on CFD in Ship Hydrodynamics, Gothenburg 2000. SRI was asked to provide validation data for this ship to the workshop. The purpose of this investigation is to quantify and to report uncertainties in the surface pressure and local velocity field measurements around a modern and practical hull form ship with a bulbous bow, stern bulb and transom stern.

The information on geometrical shape and the experimental conditions of a KCS model [4] was provided by KRISO. The ship model was manufactured at SRI's model workshop based on the lines drawn by KRISO and a Japanese company.

All of the measurements, that is, resistance and self-propulsion tests [5], wave profile measurement [6], surface pressure measurement [7], local velocity field measurement [8], propeller open test [9], were performed at the SRI 400m towing tank. The propeller model, SRI M. P. No.460, was offered from KRISO to use for self-propulsion tests, hull surface pressure and local velocity field measurements, while SRI M.P.No.465 was manufactured at Ship Research Center (SRC) based on the offsets provided by KRISO. The surface pressure measurements were conducted on the hull surface near the stern from the square station, S.S. 3 to S.S. 1/2 on the port side and SS. 2 to 1 on the starboard side. The measurements were performed not only under the "propeller working condition" at "ship point" but also under the "without propeller condition". The local velocity field measurements were conducted at two stations around the stern including the propeller plane. One of the measurements was performed immediately behind the propeller, that is, 0.25 diameters downstream of the propeller plane under a propeller operating condition.

The method used in the present uncertainty analysis mainly follows the uncertainty assessment methodology described in the procedure 4.9-03-01-01 of ITTC, which is based on the American National Standards Institute (ANSI) and American Society of Mechanical Engineers (ASME) standard on measurement uncertainty (1985) [10] and the American Institute of Aeronautics and Astronauts (AIAA) standard (1995) [11]. In the present analysis, these

standards were referred to identify the sources of error, which affected the total uncertainty in the measurements and to examine the overall level of uncertainty in the measurements during above-mentioned tests. The aim of this project was to employ the results to reduce future uncertainty levels in the experiments at SRI and to provide a starting point for uncertainty analysis.

The uncertainty analysis for measurement results obtained through the present careful experiments is expected to provide valuable information for the entire CFD and EFD community.

2. Experimental Setup

2.1 Ship Model

The principal particulars and the geometrical hull form shape of the ship model, SRI M. S. No. 631 are given in **Table 1** and **Fig. 1**, respectively. The ship model was manufactured to the same size as that used at KRISO, and was made of a combination of paraffin and wood.

The lines of this ship model was slightly modified and drawn by SRI and a Japanese company based on the lines provided by the KRISO with a scale ratio of 31.5994, so as to be able to manufacture the model in the SRI model workshop. A noticeable difference in the lines drawn at SRI and KRISO could be observed mainly around the bulbous bow and flat stern hull above the propeller.

Unfortunately the ship model made at SRI shrank non-uniformly by about 5mm in the longitudinal direction, especially around the aft body. The deformation in other directions was within 1mm and occurred primarily during the first measurement at SRI 400m towing tank. In spite of slight modification of the lines and deformation of the ship model, reasonable correlation on the local velocity field measurements at the propeller plane was found between the data obtained at SRI and KRISO [4].

The square station described in this report is defined as the length between the fore and the aft perpendiculars divided by ten, and the aft and the fore perpendiculars are denoted as S.S. 0 and 10, respectively. The maximum sectional area of this ship is located at S.S. 4 3/4, not at the midship, that is, S.S. 5.

Studs with trapezoidal heads for turbulence stimulation were placed at S.S. 9 1/2 and the middle of the bow bulb with 10mm intervals to make the flow around the hull fully turbulent. The height and front width of studs were 1.5mm. The rudder shape was simplified as shown in **Fig. 1** but not attached during the present measurements.

This ship model was also used for resistance tests [5], self-propulsion tests [5], wave profile measurements [6], local velocity field measurements [8], and surface pressure measurements [7]. For surface pressure measurements, 164 pressure taps and 73 taps were placed on the hull mainly from S.S. 3 to 1/4 on the port side of the model and mainly from S.S. 2 to 1 on the port side respectively, but 144 pressure taps were used at each measurement.

2.2 Propeller Model

The principal particulars and the geometrical shape of the propeller model, SRI M. P. No. 460 (KRISO KP505) are given in **Table 2** and **Fig. 2** respectively. This model was manufactured by KRISO and sent to SRI for rental use. The propeller open water characteristics were also measured at SRI [9]. The measured thrust K_T and torque K_Q at SRI are larger than those measured at KRISO at the same advance ratio J [7,8,9]. The propeller model was equipped at $x/L=0.4825$, that is, $0.0175L$ (127.3mm) upstream from A.P.

2.3 Experimental Apparatus

The measurements were performed at the SRI 400m towing tank with dimensions of 400m in length, 18m in breath and 8m in depth. The maximum speed of the towing carriage is currently around 12m/s. The adjustment of the draft of this ship model was made in the trimming tank through glass windows.

For surface pressure measurements on the hull surface near the stern, 144 pressure taps were employed. The diameters of the pressure tap head and the hole are 6mm and 1mm, respectively. The calibration of pressure transducers was carried at the SRI 400m towing tank at the beginning and the end of each day. The present calibration was simply carried out changing the vertical position of pressure transducers from -40 to 40 mm.

For the three-dimensional velocity field measurements around the stern, an eight-hole spherical type Pitot tube was used. The diameters of the probe and each hole are 8mm and 0.6mm, respectively. The calibration of the Pitot tube was carried at the SRI 400m towing tank. The present calibration was carried out by simply changing the angle of the Pitot tube relative to the vertical and horizontal directions separately. The Pitot tube was calibrated at 48 angles in the range from -35 to 60 degree pitch and from -35 to $+35$ degree yaw, keeping the other angles zero. Such a calibration was not sufficient to get accurate calibration curves for the eight-hole Pitot tube used for local velocity field measurements. The calibration coefficients to determine the magnitudes and angles of local flow for the current experiment were used by assuming a similarity in each coefficient, but they will be improved in the future. A two-dimensional traversing system was installed on the ship model and one Pitot tube scanned the vertical planes including the propeller disk. This device was equipped with a balancing weight to prevent heel of the ship model due to the traverse of a Pitot tube.

Pressure taps were connected to six semi-conductor type pressure transducers (Toyoda PD104W, capacity; 3,000mmAq) by vinyl tubes through six scanning valves (W0602/1P-24T). Other two pressure transducers were employed to measure the pressure at the bottom of the ship model and static pressure at a reference Pitot tube. The eight-hole Pitot tube was connected to each pressure transducer by vinyl tubing of which inner and outer diameters were 1.6 and 2.0 mm, respectively. Eight semi-conductor type pressure transducers (Toyoda PD104, capacity; 3,000mmAq) were used and connected to separate amplifiers.

The pressure signals were amplified 2,000 times for surface pressure measurements and 500 or 1,000 times for local velocity measurements by eight measuring amplifiers (Toyoda AA3004 and AA3000). The cut-off frequency of the low pass filters (Kyowa LFV-21A) was set to 10Hz for surface pressure measurements and 20Hz for local velocity field measurements. The filtered signals were monitored by a multi-pen recorder (Graphtec MC 6625) and the un-filtered pressure signals were recorded by an analogue data recorder (Kyowa RTP-650B) at a tape speed of 1.2cm/s and over a frequency range of DC to 625Hz.

The data acquisition of mean pressure was made by a personal computer (HP Vectra) through an A/D signal board (National Instrument, ± 10 Volt, 16bits) where the sampling rate and period were 20Hz and 7 seconds, respectively. The data acquisition of mean velocities was made by a personal computer through an A/D signal board where the sampling rate and period were 100Hz and 5 seconds, respectively. The measured signal was simply averaged and normalized by the ship model speed to the ground U .

In order to correct for the effect of variation in the rail height and water level during the measurements, a reference Pitot tube was utilized. To measure the relative speed of the ship model to tank water during each run, a turbine meter was set 171mm below the tank water level corresponding to half of the draft and 10.9m in front of the ship model

3. Experimental Procedure and Conditions

The measurements of wave profile and local velocity field on the KCS model were carried out at the KRISO towing tank under fixed conditions [4]. The trim and sinkage of the ship model were not allowed at the given draft using two clamping devices. This method could not be adopted to the measurements at the SRI 400m towing tank due to a leakage of tank water.

In order to conduct the present measurements under similar experimental conditions to the KRISO measurements of resistance, self-propulsion, wave profile and local velocity field, the initial trim and weight arrangement were sought by a trial and error method to realize zero trim and sinkage of the ship model in a free running condition. This condition of the ship model was called the even keel condition. The carriage speed relative to the ground was kept at 2.196m/s corresponding to $Fr=0.2600$ under the even keel condition.

In surface pressure measurements, eight sets of measurement data could be obtained by changing the scanning valves during one carriage run, that is, 48 data points could be measured at each run. Therefore, the surface pressure measurements at 144 points could be accomplished by three carriage runs. Three repeat tests were made for each condition. The measurements were performed by adjusting the displacement of the model to the given value, 1,644.0kg. Measurements at 7 to 11 positions were possible during one carriage run.

All of the measurements were performed without a rudder. Under the resistance test condition, that is, the without propeller condition for surface pressure measurements, total resistance coefficient C_{TM} and residuary resistance coefficient C_R were measured to be 0.003519

and 0.0006888, respectively. Reynolds number, Re for surface pressure measurements was 1.406×10^7 at 15.1°C . Under the without propeller condition for local velocity field measurements, total resistance coefficient C_{TM} was estimated to be 0.003534 from the resistance tests. Re for local velocity field measurements was 1.362×10^7 at 13.9°C . The density of tank water ρ was assumed to be $101.88\text{kg}\cdot\text{s}^2/\text{m}^4$ in this report.

In both measurements under the propeller working condition, the revolution rate of the propeller model was set to 9.5rps with an even keel and the ship model was self-propelled at the “ship point”, that is, the ship self-propulsion condition. The thrust K_T and torque K_Q coefficients were 0.1703 and 0.02880, respectively. The thrust loading coefficient C_{Th} and advance coefficient J were estimated to be 0.5074 and 0.728 from the propeller open water characteristics curves measured by SRI [7,8,9]. Reynolds number under the propeller working condition for surface pressure measurements was 1.402×10^7 at 15.0°C and the same as that under the without propeller condition, while Re under the propeller working condition for local velocity measurements was 1.348×10^7 at 13.5°C and slightly different from that under the without propeller condition.

Repeated measurements for local velocity field measurements were performed at $Re=1.273 \times 10^7$ and 11.4°C under the without propeller condition, and at $Re=1.252 \times 10^7$ and 11.5°C under the with propeller working condition in April 2000.

4. Uncertainty Analysis for Surface Pressure Measurement

The surface pressure measurements were performed in December 1999 and March 2000. The repeated measurements were performed only in March 2000. In this report, the average values and precision limit were calculated only with the measurements conducted in March 2000. Six representative measuring points where the pressure taps were equipped most precisely were selected for the present uncertainty analysis. The positions of these sampling points were shown in **Table 3**

4.1 Identified Source of Errors

Concerning bias limit, the standard errors of estimate (SEE) on each linear calibration curve for pressure transducers and the error of carriage speed to the ground used for non-dimensionalization of pressure coefficients were considered, while concerning precision limit, the standard deviations obtained from multiple test data and the error of carriage speed to the ground were used. The influence of equipment accuracy of pressure taps to the pressure coefficient was not considered, because the sensitivity coefficients were not known at this moment. Then, the data at the most accurately equipped pressure taps were evaluated in the present uncertainty analysis.

The other error sources were not considered because those were expected to be negligible.

4.1.1 Bias Error Estimated from SEE of Pressure Transducers

From the calibration of pressure transducers performed at the beginning of each test day, the standard error of estimate (SEE) was calculated. The bias limits result from approximating the calibration curve by a linear regression fitting and ± 2 SEE band about the regression curve is a confidence level in the curve fitting. The sensitivity coefficient to the pressure coefficient due to the standard error of estimate $\theta^{C_p}_{SEE}$ and the bias limits to the pressure coefficient due to the standard error of estimate $B^{SEE}_{C_p}$ are calculated by the following equations.

$$\begin{aligned}
 SEE &= \sqrt{\sum_{j=1}^N \{Y_j - (aX_j + b)\}^2 / (N - 2)} \\
 B_{SEE} &= \pm 2 \times SEE \\
 \theta^{C_p}_{SEE} &= \partial C_p / \partial SEE = 2g/V_e^2 \\
 B^{SEE}_{C_p} &= \theta^{C_p}_{SEE} \times B_{SEE}
 \end{aligned}$$

where

- Y_j : Measured Value
- N : Number of Measurements
- a : Slope of Calibration Curve
- b : Intercept at y ordinate

The bias errors for each pressure transducer for the without propeller and with working propeller conditions are shown in **Table 4**

4.1.2 Bias Error due to Residual Current

The pressure coefficients are non-dimensionalized by the carriage speed to the ground in this report. Using the measured the carriage speed to the tank water by a current meter in the resistance test in December, 1999, the bias errors due to the residual current B_{V_e} and the precision limit due to the residual current S_{V_e} can be estimated as follows,

$$B_{V_e} = -0.014 \text{ and } +0.003,$$

$$S_{V_e} = 0.0037$$

The sensitivity coefficients to the pressure coefficient due to the error of carriage speed to the ground, $\theta^{C_p}_{V_e}$, the bias errors and precision errors due to residual current under the without and with working propeller conditions are given in **Tables 5(a)** and **(b)**.

4.1.3. Precision Error Estimated from Multiple Runs

The average values and precision limit for the without propeller and with working propeller conditions through multiple measurements are shown in **Tables 6(a)** and **(b)**. In order to calculate the standard deviation at each pressure tap, the following equation was used.

$$S_X = \sqrt{\sum_{j=1}^N (X_j - \bar{X})^2 / (N - 1)} \quad (1)$$

where

\bar{X} : Average of Measured Variables X_j

4.2 Bias limit, Precision Limit and Uncertainty on Surface Pressure Measurement

Repeated measurements were performed from six to nine runs. The use of the coverage factor of $K=2$ assumes a large sample size and Gaussian error distribution. Since the bias and precision limits had similar magnitude in the present measurements, the use of $K=2$ was permissible. The bias limit, precision limit and comprehensive uncertainty U_{Cp} with a 95% confidence level are shown in **Tables 7(a)** and **(b)**.

5. Uncertainty Analysis for Local Velocity Field Measurement

The local velocity field measurements were carried out in December, 1999 and April, 2000. Repeated measurements were conducted only in April, 2000. The measured data in December, 1999 and in April, 2000 were used for the average values and precision limit, respectively. The sampling positions used for the present uncertainty analysis are shown in **Table 8**

5.1 Equation of Local Velocities

Three-dimensional velocities of the inflow coming from the direction of positive β_v and β_h can be calculated by the following equations.

$$\begin{aligned} u &= (V_v \cos \beta_v + V_h \cos \beta_h) / 2 \\ v &= V_h \sin \beta_h \\ w &= V_v \sin \beta_v \end{aligned}$$

where

$$\begin{aligned} V_v &= \sqrt{|2(H_C - H_B) / (c_0 + c_1 \cdot \beta_v + c_2 \cdot \beta_v^2 + c_3 \cdot \beta_v^3)|} \\ V_h &= \sqrt{|2(H_C - H_P) / (d_0 + d_1 \cdot \beta_h + d_2 \cdot \beta_h^2 + d_3 \cdot \beta_h^3)|} \\ \beta_v &= a_0 + c_1 \cdot F_v + a_2 \cdot F_v^2 + a_3 \cdot F_v^3 \\ \beta_h &= b_0 + b_1 \cdot F_h + b_2 \cdot F_h^2 + b_3 \cdot F_h^3 \\ F_v &= (H_T - H_B) / (2H_C - H_T - H_B) \\ F_h &= (H_S - H_P) / (2H_C - H_S - H_P) \end{aligned}$$

where $a_0, a_1, a_2, a_3, b_0, b_1, b_2, b_3, c_0, c_1, c_2, c_3, d_0, d_1, d_2, d_3$ are the linear regression coefficients. H_T, H_B and others are the head of each pressure hole of a spherical type eight-hole Pitot tube as shown in **Fig. 3**

5.2 Identified Source of Errors

Concerning the bias errors, standard error estimates of calibration curve fitting of pressure transducers and the calibration curve fitting of an eight-hole Pitot tube were considered, while concerning precision limit, standard deviations obtained from multiple test data were used. The error due to the residual current was not considered because the velocities were non-dimensionalized by the carriage speed to the tank water.

The sources of other errors were not estimated because they were expected to be negligible.

5.2.1 Bias Error Estimated from SEE of Pressure Transducers

From the calibration of pressure transducers performed at the beginning of each test day, standard error estimate (SEE) was calculated. The bias limit results from approximating the calibration with a linear regression curve fit and ± 2 SEE band about the regression curve is a confidence level on the curve fit. Since the measurements were performed during more than two days, more than two calibration data for each transducer exist and then the biggest errors were used as the bias error of each transducer. The bias errors for each pressure hole and the sensitivity coefficient to local velocities are denoted as B_{SEE}^{HT} , B_{SEE}^{HB} , ..., B_{SEE}^{HP1} and θ_{SEE}^u , θ_{SEE}^v , θ_{SEE}^w . Then, the bias errors of u, v, w given by SEE can be calculated by the following equations.

$$\begin{aligned}
 B_{F_v} &= \sqrt{(\theta_{H_T}^{F_v} B_{SEE}^{H_T})^2 + (\theta_{H_B}^{F_v} B_{SEE}^{H_B})^2 + (\theta_{H_C}^{F_v} B_{SEE}^{H_C})^2} \\
 B_{F_h} &= \sqrt{(\theta_{H_S}^{F_h} B_{SEE}^{H_S})^2 + (\theta_{H_P}^{F_h} B_{SEE}^{H_P})^2 + (\theta_{H_C}^{F_h} B_{SEE}^{H_C})^2} \\
 B_{\beta_v} &= \theta_{F_v}^{\beta_v} B_{F_v} \\
 B_{\beta_h} &= \theta_{F_h}^{\beta_h} B_{F_h} \\
 B_{V_v} &= \theta_{\beta_v}^{V_v} B_{\beta_v} \\
 B_{V_h} &= \theta_{\beta_h}^{V_h} B_{\beta_h} \\
 B_u &= \sqrt{(\theta_{\beta_v}^u B_{\beta_v})^2 + (\theta_{\beta_h}^u B_{\beta_h})^2 + (\theta_{V_v}^u B_{V_v})^2 + (\theta_{V_h}^u B_{V_h})^2} \\
 B_v &= \sqrt{(\theta_{\beta_h}^v B_{\beta_h})^2 + (\theta_{V_h}^v B_{V_h})^2} \\
 B_w &= \sqrt{(\theta_{\beta_v}^w B_{\beta_v})^2 + (\theta_{V_v}^w B_{V_v})^2}
 \end{aligned}$$

where

$$\begin{aligned}
 \theta_{H_T}^{F_v} &= 1/(2H_C - H_T - H_B) + (H_T - H_B)/(2H_C - H_T - H_B)^2 \\
 \theta_{H_B}^{F_v} &= -1/(2H_C - H_T - H_B) + (H_T - H_B)/(2H_C - H_T - H_B)^2 \\
 \theta_{H_C}^{F_v} &= -2(H_T - H_B)/(2H_C - H_T - H_B)^2 \\
 \theta_{H_S}^{F_h} &= 1/(2H_C - H_S - H_P) + (H_T - H_B)/(2H_C - H_S - H_P)^2 \\
 \theta_{H_P}^{F_h} &= -1/(2H_C - H_S - H_P) + (H_T - H_B)/(2H_C - H_S - H_P)^2 \\
 \theta_{H_C}^{F_h} &= -2(H_S - H_P)/(2H_C - H_S - H_P)^2 \\
 \theta_{F_v}^{\beta_v} &= a_1 + 2a_2 F_v + 3a_3 F_v^2 \\
 \theta_{F_h}^{\beta_h} &= b_1 + 2b_2 F_h + 3b_3 F_h^2
 \end{aligned}$$

$$\begin{aligned}
\theta_{\beta_v}^{V_v} &= -\sqrt{|H_C - H_B|}(c_1 + 2c_2\beta_v + 3c_3\beta_v^2)/\sqrt{2}(c_0 + c_1\beta_v + c_2\beta_v^2 + c_3\beta_v^3)^{3/2} \\
\theta_{\beta_h}^{V_h} &= -\sqrt{|H_C - H_P|}(d_1 + 2d_2\beta_h + 3d_3\beta_h^2)/\sqrt{2}(d_0 + d_1\beta_h + d_2\beta_h^2 + d_3\beta_h^3)^{3/2} \\
\theta_{\beta_v}^u &= -0.5V_v \sin \beta_v \\
\theta_{\beta_h}^u &= -0.5V_h \sin \beta_h \\
\theta_{V_v}^u &= 0.5 \cos \beta_v \\
\theta_{V_h}^u &= 0.5 \cos \beta_h \\
\theta_{\beta_h}^v &= V_h \cos \beta_h \\
\theta_{V_h}^v &= \sin \beta_h \\
\theta_{\beta_v}^w &= V_v \cos \beta_v \\
\theta_{V_v}^w &= \sin \beta_v
\end{aligned}$$

The bias errors for each pressure transducer under the without propeller and with working propeller conditions are shown in **Table 9**

5.2.2 Precision Error Estimated from Multiple Runs

The average values of local velocities at nine sampling points and precision limit for the without propeller and with working propeller conditions through multiple measurements are shown in **Tables 10 (a)** and **(b)**. To calculate the standard deviation at each pressure taps, the equation (1) was used.

5.2.3. Bias Error Estimated from Calibration Curve Fitting

By calculating three-dimensional local velocities at the calibration with the calibration curves for an eight-hole Pitot tube, the maximum errors of each local non-dimensionalized velocity u, v, w were estimated as follows

$$\begin{aligned}
u &= 0.0106 \text{ and } -0.0470 \\
v &= 0.0134 \text{ and } -0.0058 \\
w &= 0.0132 \text{ and } -0.0087
\end{aligned}$$

These errors were considered as the bias errors of each velocity B^{fit}_u , B^{fit}_v , and B^{fit}_w due to calibration curve fitting of an eight-hole Pitot tube.

5.3 Bias limit, Precision Limit and Uncertainty on Local Velocity Field Measurement

Since the repeated measurements were performed with ten runs, the coverage factors of $K=2$ was used. The bias limit, precision limit and comprehensive uncertainty with a 95% confidence level are shown in **Tables 11(a)** and **(b)**.

6. Concluding Remarks

This report describes the results of uncertainty analysis of surface pressure and local

velocity field measurements around a modern and practical 3,600TEU KRISO container ship (KCS) model. Uncertainties were estimated for major sources of errors, which affect remarkably. In the present uncertainty analysis, all of significant sources of the errors were not considered. Further repeat measurements are needed to confirm the present analysis.

The measurements on a KCS model were performed both the without the propeller and with working propeller under the even keel condition. It is expected that the data will be useful for validating CFD computations.

Acknowledgement

The authors wish to express their gratitude to Dr. Yang, S.I., Dr. Van, H.S. and Dr. Kim, W.J. for their kind cooperation in providing us with the lines and the offsets of the KCS, lending the propeller model and discussing the measurements.

The authors thank Dr. Fuwa, T. for his encouragement and Mr. Hasegawa, J., Mr. Yanagihara, Mr. T., Fukasawa R., and those members of the staff at the Ship Research Institute for their sincere support during the experiment and manufacture of the ship model.

References

1. The Resistance Committee, "Final Report and Recommendations to the 22nd ITTC of Resistance Committee", Proc. of 22nd ITTC, Vol. 1, Seoul/Shanghai (1998), pp. 173-246.
2. Kume, K., Hirata, N., Hasegawa, J., Tsukada, T., Hinatsu, M., "An Uncertainty Analysis for Towing Tank Tests with a Full Form Ship Model", Proc. of 73rd General Meeting of Ship Research Institute (1999) [In Japanese].
3. Kume, K., Hirata, N., Hasegawa, J., Tsukada, T., Hinatsu, M., "An Uncertainty Analysis Method for Ship Model", Report of SRI (to be published), [In Japanese].
4. Van, S.H., Kim, W.J., Yim, G.T., Kim, D.H., and Lee, C.J., "Experimental Investigation of the Flow Characteristics around Practical Hull Forms", Proc. of the 3rd Osaka Colloquium on Advanced CFD Applications to Ship Flow and Hull Form Design, Osaka (1998), pp. 215-227.
5. Hasegawa, J. et al., "Resistance Tests and Self-Propulsion Tests on the KCS Model in the SRI 400m Towing Tank", SPD Report No. 00-006-01, Ship Performance Division, Ship Research Institute (2000, in Preparation).
6. Hori, T. et al., "Wave Profile Measurement around the KCS Model in the SRI 400m Towing Tank", SPD Report No. 00-007-01, Ship Performance Division, Ship Research Institute (2000, in Preparation).
7. Tsukada, Y. et al., "Surface Pressure Measurements on the KCS in the SRI 400m Towing Tank", SPD Report No. 00-004-01, Ship Performance Division, Ship Research Institute (2000, in Preparation).
8. Fujisawa, J. et al., "Local Velocity Measurements around the KCS Model in the SRI 400m

- Towing Tank”, SPD Report No. 00-003-02, Ship Performance Division, Ship Research Institute (2000).
9. Ukon, Y. et al., “Propeller Open Water Characteristics of the KCS Model Propeller”, SPD Report No. 00-005-01, Ship Performance Division, Ship Research Institute (2000, in Preparation)
 10. ANSI/ASME, ”Measurement Uncertainty: Part 1, Supplement on Instruments and Apparatus”, ANSI/ASME PTC 19.I-1985 , JSME (1985)) [In Japanese].
 11. AIAA, “Assessment of Wind Tunnel Data Uncertainty”, AIAA S-071-1995 (1995).

Nomenclatures

A_M	Midship Section Area [m ²]
A_0	Propeller Disk Area [m ²], $=(\pi D_p^2)/4$
a_E	Expanded Area Ratio [-]
B	Breadth of Ship [m]
C_B	Block Coefficient [-]
C_F	Frictional Resistance Coefficient [-], $=R_F/(1/2\rho U^2 S_w)$
C_M	Midship Section Coefficient [-], $=A_M/BT$
C_P	Pressure Coefficient [-], $=(P - P_0)/(1/2\rho U^2)$
C_P	Prismatic Coefficient [-], $=\nabla/(A_M L_{PP})$
C_R	Residuary Resistance Coefficient [-], $=R_R/(1/2\rho U^2 S_w)$
C_{Th}	Thrust Loading Coefficient [-], $=T/(1/2\rho U^2 A_0)$
C_{TM}	Total Resistance Coefficient [-], $=R_{TM}/(1/2\rho U^2 S_w)$
D	Depth of Ship [m]
D_p	Propeller Diameter [m]
d	Draft of Ship [m]; T
F_h, F_{h8}	Function to determine Horizontal components of Flow Angle for Each Five-Hole System [-]
F_v, F_{v8}	Function to determine Vertical components of Flow Angle for Each Five-Hole System [-]
F_r	Froude Number Based on Length between Perpendiculars, L ; $F_n = U/(gL)^{1/2}$
G_h, G_{h8}	Function to determine Horizontal component of Inflow Velocity [-]
G_v, G_{v8}	Function to determine Vertical component of Inflow Velocity [-]
g	Acceleration of Gravity [m/s ²]
$H_T, H_B, H_C, H_P, H_S, H_{T1}, H_{P1}, H_{S1}$	Head at Each Pressure Hole, T, B, C, P, S, T_1, P_1 and S_1 of Eight-Hole Spherical Type Pitot Tube [Aq]
I	Propeller Immersion [m]
J	Advance Coefficient [-], $=V_A / n_P D$
K_Q	Torque Coefficient [-], $=Q/\rho n_P^2 D^5$
K_T	Thrust Coefficient [-], $=T/\rho n_P^2 D^4$
L	Length between Perpendiculars [m]; L_{PP}
L_{PP}	Length between Perpendiculars [m]; L
L_{WL}	Length at Load Water Line [m]
l_{CB}	Center of Buoyancy from Midship [% L_{PP} , Backward +]
N	Number of Individual Readings [-]
n_P	Propeller Revolution Rate [1/s, Hz]
P	Pressure [kg/ m ²]

P_0	Reference Pressure at Infinity [kg/ m^2]
p	Pitch Ratio [-]
Re	Reynolds' Number Based on Length between Perpendiculars [-]
R_F	Frictional Resistance [kg]
R_R	Residuary Resistance [kg]
R_T	Total Resistance [kg]
S_R	Wetted Surface Area of Rudder [m^2]
S_W	Wetted Surface Area of Naked Hull without Rudder [m^2]
T	Draft of Ship [m]; d
T_W	Temperature of Tank Water [$^{\circ}\text{C}$]
U	Speed of Ship Model [m/s]
u,v,w	Local Mean-Velocities in (x,y.z) directions
V_A	Propeller Advance Speed [m/s]; $=(1-w_T)U$
V_e	Speed of Ship Model to the Ground [m/s]
V_h	Horizontal Component of Inflow Velocity to Pitot Tube [m/s]
V_v	Vertical Component of Inflow Velocity to Pitot Tube [m/s]
w_T	Axial Wake Fraction determined by Propeller Thrust [-]
x	Coordinate for Longitudinal Direction of Ship [m]
x_B	Propeller Boss Ratio [-]
y	Coordinate for Transverse Direction of Ship [m]
Z	Number of Blade [-]
z	Coordinate for Vertical Direction of Ship [m]
β_h	Flow Angle between Horizontal Component of Inflow and X-Axis [deg]
β_v	Flow Angle between Vertical Component of Inflow and X-Axis [deg]
η_o	Propeller Efficiency [-]; $=(JK_T)/(2 K_Q)$
Θ_R	Rake Angle [deg]
Θ_S	Skew Angle [deg]
θ	Sensitivity Coefficient
ν	Coefficient of Kinematic Viscosity [m^2/s]
ρ	Density of Water [$\text{kg}\cdot\text{s}^2/\text{m}^4$]
V	Displacement Volume of Ship Model [m^3]

Table 1 Principal Particulars of Tested Ship

Ship Model Name			KRISO Container Ship
SRI M. S. No.			631
KRISO M. S. No.		m	KS621
Length between Perpendiculars	L _{PP}	m	7.2786
Length of Load Water Line	L _{WL}	m	7.3568
Breadth (Moulded)	B	m	1.0190
Depth (Moulded)	D	m	0.5696
Draft (Moulded)	d	m	0.3418
Wetted Surface Area w/o Rudder*	S _W	m ²	9.4984
Rudder Surface Area	S _R	m ²	0.0741
Displacement w/o Rudder*	∇	m ³	1.6497
Center of Buoyancy from Midship (Backward, +) *	l _{CB}	% L _{PP}	1.48
Blockage Coefficient*	C _B	-	0.6508
Midship Coefficient*	C _M	-	0.9849
Prismatic Coefficient*	C _P	-	0.6608

* These values were calculated by Japanese Company

Table 2 Principal Particulars of Tested Propeller

Propeller Name			KCS Propeller	
SRI M. P. No.			460	465
KRISO M. P. No.			KP505	-
Diameter	D _P	m	0.2500	
Boss Ratio	x _B	-	0.1800	
Pitch Ratio at 0.7R	p	-	0.9967	
Expanded Blade Area Ratio	a _E	-	0.800	
Rake Angle	Θ _R	deg	0.000	
Skew Angle	Θ _S	deg	32.0	
Number of Blade	Z	-	5	
Direction of Rotation			Right	
Blade Section			NACA66 Thickness +a=0.8 Camber	

Table 3 Position of Pressure Taps

Press.Tap No.	$x[mm]$	$y[mm]$	$z[mm]$	S.S.	W.L.	Press.Transducer No.
P.T.No.1	2181.81	-345.84	-158.20	2	5	PT-1
P.T.No.2	2544.09	-0.02	-0.47	1.5	0	PT-3
P.T.No.3	2545.59	-147.60	-62.08	1.5	2	PT-3
P.T.No.4	2544.90	-259.45	-189.15	1.5	6	PT-3
P.T.No.5	2726.15	-184.40	-189.24	1.25	6	PT-4
P.T.No.6	2907.34	-217.55	-252.56	1	8	PT-6

Table 4 Bias Error of Pressure Transducer Calibration

w/o Propeller					
Mar.23	Slope[$mmAq/bit$]	Intercept[$mmAq$]	$SEE[mmAq]$	$B_{SEE}[mmAq]$	$B_{C_p}^{SEE}$
PT-1	0.012489	-1.9725	0.2277	0.4554	0.0019
PT-2	0.014826	5.6715	0.1416	0.2832	0.0012
PT-3	0.012957	0.4980	0.3258	0.6516	0.0027
PT-4	0.014794	-4.5125	0.1705	0.3410	0.0014
PT-5	0.015046	0.4169	0.4396	0.8792	0.0036
PT-6	0.009126	-2.3782	0.0452	0.0904	0.0004
w/ Propeller					
Mar.24	Slope[$mmAq/bit$]	Intercept[$mmAq$]	$SEE[mmAq]$	$B_{SEE}[mmAq]$	$B_{C_p}^{SEE}$
PT-1	0.012083	1.7924	0.1381	0.2762	0.0011
PT-2	0.014767	1.3326	0.1282	0.2564	0.0010
PT-3	0.012465	1.5526	0.1628	0.3256	0.0013
PT-4	0.014709	0.8115	0.0983	0.1966	0.0008
PT-5	0.014618	1.2107	0.3333	0.6666	0.0027
PT-6	0.009174	-0.3454	0.0507	0.1014	0.0004

Table 5(a) Estimated Errors due to Residual Current, without Propeller

	P.T.No.1	P.T.No.2	P.T.No.3	P.T.No.4	P.T.No.5	P.T.No.6
$B_{V_e}^+$	0.003	0.003	0.003	0.003	0.003	0.003
$B_{V_e}^-$	0.014	0.014	0.014	0.014	0.014	0.014
S_{V_e}	0.004	0.004	0.004	0.004	0.004	0.004
$\theta_{V_e}^{C_p}$	0.112	0.058	0.101	0.061	0.036	-0.013
$B_{C_p}^{V_e+}$	0.0003	0.0002	0.0003	0.0002	0.0001	0.0000
$B_{C_p}^{V_e-}$	0.0016	0.0008	0.0014	0.0009	0.0005	0.0002
S_{C_p}	0.0004	0.0002	0.0004	0.0002	0.0001	0.0001

Table 5(b) Estimated Errors due to Residual Current, with Working Propeller

	P.T.No.1	P.T.No.2	P.T.No.3	P.T.No.4	P.T.No.5	P.T.No.6
$B_{V_e}^+$	0.003	0.003	0.003	0.003	0.003	0.003
$B_{V_e}^-$	0.014	0.014	0.014	0.014	0.014	0.014
S_{V_e}	0.004	0.004	0.004	0.004	0.004	0.004
$\theta_{V_e}^{C_p}$	0.109	0.062	0.106	0.065	0.043	0.000
$B_{C_p}^{V_e+}$	0.0003	0.0002	0.0003	0.0002	0.0001	0.0000
$B_{C_p}^{V_e-}$	0.0015	0.0009	0.0015	0.0009	0.0006	0.0000
S_{C_p}	0.0004	0.0002	0.0004	0.0003	0.0002	0.0000

Table 6(a) Estimated Precision Limits of Pressure Coefficient, without Propeller

w/o Propeller						
Run No.	P.T.No.1	P.T.No.2	P.T.No.3	P.T.No.4	P.T.No.5	P.T.No.6
1st	-0.1278	-0.0677	-0.1088	-0.0819	-0.0533	0.0040
2nd	-0.1252	-0.0670	-0.1066	-0.0671	-0.0384	0.0135
3rd	-0.1249	-0.0592	-0.1100	-0.0660	-0.0394	0.0159
4th	-0.1257	-0.0623	-0.1158	-0.0644	-0.0373	0.0161
5th	-0.1199	-0.0666	-0.1088	-0.0660	-0.0398	0.0120
6th	-0.1218	-0.0622	-0.1142	-0.0688	-0.0419	0.0124
7th	-0.1161			-0.0701	-0.0407	0.0114
8th	-0.1205			-0.0655	-0.0372	0.0157
9th				-0.0692	-0.0401	0.0127
Average	-0.1227	-0.0642	-0.1107	-0.0690	-0.0409	0.0127
Standard Deviation	0.0038	0.0034	0.0036	0.0020	0.0016	0.0019

Table 6(b) Estimated Precision Limits of Pressure Coefficient, with Working Propeller

w/ Propeller						
Run No.	P.T.No.1	P.T.No.2	P.T.No.3	P.T.No.4	P.T.No.5	P.T.No.6
1st	-0.1243	-0.0707	-0.1226	-0.0741	-0.0486	0.0011
2nd	-0.1207	-0.0729	-0.1202	-0.0699	-0.0442	-0.0108
3rd	-0.1187	-0.0669	-0.1182	-0.0714	-0.0481	0.0018
4th	-0.1175	-0.0693	-0.1157	-0.0715	-0.0473	0.0024
5th	-0.1174	-0.0633	-0.1151	-0.0701	-0.0456	0.0051
6th	-0.1205	-0.0685	-0.1124	-0.0730	-0.0480	0.0023
7th	-0.1155	-0.0672	-0.1166	-0.0693	-0.0453	0.0003
8th	-0.1188	-0.0684	-0.1134	-0.0729	-0.0485	0.0015
9th						0.0003
Average	-0.1192	-0.0684	-0.1168	-0.0715	-0.0469	0.0005
Standard Deviation	0.0027	0.0028	0.0034	0.0017	0.0017	0.0045

Table 7(a) Bias Limits, Precision Limits and Uncertainties, without Propeller

Items	P.T.No.1	P.T.No.2	P.T.No.3	P.T.No.4	P.T.No.5	P.T.No.6
$B_{C_p}^{SEE}$	0.0019	0.0012	0.0027	0.0014	0.0036	0.0004
$B_{C_p}^{V_e^+}$	0.0003	0.0002	0.0003	0.0002	0.0001	0.0000
$B_{C_p}^{V_e^-}$	0.0016	0.0008	0.0014	0.0009	0.0005	0.0002
$S_{C_p}^{V_e}$	0.0004	0.0002	0.0004	0.0002	0.0001	0.0001
$S_{C_p}^{dispersion}$	0.0038	0.0034	0.0036	0.0020	0.0016	0.0019
$B_{C_p}^+$	0.0019	0.0012	0.0027	0.0014	0.0036	0.0004
$B_{C_p}^-$	0.0025	0.0014	0.0030	0.0017	0.0036	0.0004
S_{C_p}	0.0038	0.0034	0.0036	0.0020	0.0016	0.0019
$U_{C_p}^+$	0.0079	0.0070	0.0077	0.0043	0.0049	0.0038
$U_{C_p}^-$	0.0081	0.0070	0.0078	0.0044	0.0049	0.0038
C_p	-0.1227	-0.0642	-0.1107	-0.0690	-0.0409	0.0127

Table 7(b) Bias Limits, Precision Limits and Uncertainties, with Working Propeller

Items	P.T.No.1	P.T.No.2	P.T.No.3	P.T.No.4	P.T.No.5	P.T.No.6
$B_{C_p}^{SEE}$	0.0011	0.0010	0.0013	0.0008	0.0027	0.0004
$B_{C_p}^{V_e^+}$	0.0003	0.0002	0.0003	0.0002	0.0001	0.0000
$B_{C_p}^{V_e^-}$	0.0015	0.0009	0.0015	0.0009	0.0006	0.0000
$S_{C_p}^{V_e}$	0.0004	0.0002	0.0004	0.0003	0.0002	0.0000
$S_{C_p}^{dispersion}$	0.0027	0.0028	0.0034	0.0017	0.0017	0.0045
$B_{C_p}^+$	0.0011	0.0010	0.0013	0.0008	0.0027	0.0004
$B_{C_p}^-$	0.0019	0.0013	0.0020	0.0012	0.0028	0.0004
S_{C_p}	0.0027	0.0028	0.0034	0.0018	0.0017	0.0045
$U_{C_p}^+$	0.0055	0.0058	0.0070	0.0036	0.0043	0.0089
$U_{C_p}^-$	0.0057	0.0058	0.0072	0.0037	0.0043	0.0089
C_p	-0.1192	-0.0684	-0.1168	-0.0715	-0.0469	0.0005

Table 8 Position of Wake Measurement

	$x[mm]$	$y[mm]$	$z[mm]$
M.P.-1	3574.5	-80.0	-160.0
M.P.-2	3574.5	-60.0	-160.0
M.P.-3	3574.5	-40.0	-160.0
M.P.-4	3574.5	-20.0	-160.0
M.P.-5	3574.5	0.0	-160.0
M.P.-6	3574.5	20.0	-160.0
M.P.-7	3574.5	40.0	-160.0
M.P.-8	3574.5	60.0	-160.0
M.P.-9	3574.5	80.0	-160.0

$x = 0$: midship

Table 9 Bias Errors of Pressure Transducers

w/o Propeller				
Dec.21,22	Slope[$mmAq/bit$]	Intercept[$mmAq$]	$SEE[mmAq]$	$B_{SEE}[mmAq]$
T	0.025178	51.7391	0.3426	0.6851
B	0.024718	45.1043	0.2066	0.4131
C	0.016458	33.6302	0.4235	0.8470
S	0.017159	42.4845	0.3882	0.7765
P	0.017080	27.2786	0.2023	0.4046
T1	0.016780	21.1938	0.2177	0.4354
S1	0.025789	22.9799	0.9550	1.9101
P1	0.017955	27.3782	0.2551	0.5102
w/ Propeller				
Dec.23,24,25	Slope[$mmAq/bit$]	Intercept[$mmAq$]	$SEE[mmAq]$	$B_{SEE}[mmAq]$
T	0.050513	244.2440	0.4039	0.8077
B	0.049105	223.2686	0.2178	0.4355
C	0.033042	159.9085	0.4218	0.8437
S	0.034195	175.4304	0.3148	0.6297
P	0.034256	151.3666	0.3583	0.7166
T1	0.033413	149.1143	0.5391	1.0782
S1	0.048256	235.4803	0.7277	1.4553
P1	0.035948	167.3875	0.4280	0.8560

Table 10(a) Averaged Values of Local Velocities and Their Standard Deviations, without Propeller

w/o Propeller						
	Average			Standard Deviation		
Measuring Point	u	v	w	S_u	S_v	S_w
M.P.-1	0.8650	-0.0723	-0.1626	0.0054	0.0015	0.0014
M.P.-2	0.7409	-0.0932	-0.1272	0.0036	0.0015	0.0025
M.P.-3	0.5747	-0.0696	-0.0388	0.0077	0.0042	0.0028
M.P.-4	0.5201	-0.0366	0.0880	0.0102	0.0045	0.0042
M.P.-5	0.4609	0.0097	0.1596	0.0095	0.0041	0.0029
M.P.-6	0.5076	0.0448	0.0782	0.0091	0.0042	0.0020
M.P.-7	0.5910	0.0749	-0.0387	0.0101	0.0039	0.0030
M.P.-8	0.7357	0.0872	-0.1182	0.0086	0.0032	0.0036
M.P.-9	0.8446	0.0673	-0.1532	0.0050	0.0017	0.0020

Table 10(b) Averaged Values of Local Velocities and Their Standard Deviations, with Working Propeller

w/ Propeller						
	Average			Standard Deviation		
Measuring Point	u	v	w	S_u	S_v	S_w
M.P.-1	1.0295	-0.1751	-0.2258	0.0017	0.0007	0.0034
M.P.-2	1.0191	-0.2072	-0.2412	0.0020	0.0011	0.0029
M.P.-3	0.9700	-0.2506	-0.2105	0.0026	0.0018	0.0019
M.P.-4	0.9026	-0.2717	-0.0888	0.0040	0.0025	0.0039
M.P.-5	0.9555	-0.2767	0.1650	0.0040	0.0025	0.0056
M.P.-6	0.9828	-0.2187	0.3766	0.0033	0.0049	0.0034
M.P.-7	1.0835	-0.0868	0.1953	0.0047	0.0029	0.0049
M.P.-8	1.1528	-0.0196	0.0622	0.0049	0.0039	0.0032
M.P.-9	1.1711	0.0169	-0.0145	0.0025	0.0015	0.0026

Table 11(a) Bias Limits, Precision Limits and Uncertainties, without Propeller

Items	M.P.-1	M.P.-2	M.P.-3	M.P.-4	M.P.-5	M.P.-6	M.P.-7	M.P.-8	M.P.-9
B_u^{SEE}	0.0007	0.0008	0.0009	0.0014	0.0038	0.0016	0.0010	0.0009	0.0008
B_v^{SEE}	0.0037	0.0050	0.0066	0.0063	0.0083	0.0086	0.0084	0.0064	0.0050
B_w^{SEE}	0.0053	0.0057	0.0051	0.0115	0.0192	0.0119	0.0050	0.0055	0.0054
B_u^{fit+}	0.0106	0.0106	0.0106	0.0106	0.0106	0.0106	0.0106	0.0106	0.0106
B_u^{fit-}	0.0470	0.0470	0.0470	0.0470	0.0470	0.0470	0.0470	0.0470	0.0470
B_v^{fit+}	0.0134	0.0134	0.0134	0.0134	0.0134	0.0134	0.0134	0.0134	0.0134
B_v^{fit-}	0.0058	0.0058	0.0058	0.0058	0.0058	0.0058	0.0058	0.0058	0.0058
B_w^{fit+}	0.0132	0.0132	0.0132	0.0132	0.0132	0.0132	0.0132	0.0132	0.0132
B_w^{fit-}	0.0087	0.0087	0.0087	0.0087	0.0087	0.0087	0.0087	0.0087	0.0087
B_u^+	0.0106	0.0106	0.0106	0.0107	0.0113	0.0107	0.0106	0.0106	0.0106
B_u^-	0.0470	0.0470	0.0470	0.0470	0.0472	0.0470	0.0470	0.0470	0.0470
B_v^+	0.0139	0.0143	0.0149	0.0148	0.0158	0.0159	0.0158	0.0149	0.0143
B_v^-	0.0069	0.0077	0.0088	0.0086	0.0102	0.0104	0.0102	0.0086	0.0076
B_w^+	0.0142	0.0144	0.0141	0.0175	0.0233	0.0178	0.0141	0.0143	0.0143
B_w^-	0.0102	0.0104	0.0101	0.0144	0.0210	0.0147	0.0100	0.0103	0.0103
S_u	0.0054	0.0036	0.0077	0.0102	0.0095	0.0091	0.0101	0.0086	0.0050
S_v	0.0015	0.0015	0.0042	0.0045	0.0041	0.0042	0.0039	0.0032	0.0017
S_w	0.0014	0.0025	0.0028	0.0042	0.0029	0.0020	0.0030	0.0036	0.0020
U_u^+	0.0152	0.0129	0.0187	0.0231	0.0221	0.0212	0.0228	0.0202	0.0145
U_u^-	0.0482	0.0476	0.0495	0.0513	0.0508	0.0504	0.0512	0.0501	0.0480
U_v^+	0.0142	0.0146	0.0172	0.0174	0.0178	0.0180	0.0177	0.0162	0.0147
U_v^-	0.0074	0.0082	0.0122	0.0125	0.0131	0.0133	0.0129	0.0108	0.0084
U_w^+	0.0145	0.0152	0.0152	0.0194	0.0240	0.0182	0.0154	0.0160	0.0148
U_w^-	0.0106	0.0115	0.0115	0.0167	0.0218	0.0153	0.0117	0.0126	0.0110
u	0.8564	0.7375	0.5455	0.5000	0.4438	0.4960	0.5669	0.7317	0.8276
v	-0.0695	-0.0959	-0.0635	-0.0367	0.0043	0.0427	0.0684	0.0883	0.0649
w	-0.1644	-0.1293	-0.0400	0.0850	0.1687	0.0848	-0.0415	-0.1189	-0.1538

Table 11(b) Bias Limits, Precision Limits and Uncertainties, with Working Propeller

Items	M.P.-1	M.P.-2	M.P.-3	M.P.-4	M.P.-5	M.P.-6	M.P.-7	M.P.-8	M.P.-9
B_u^{SEE}	0.0009	0.0010	0.0012	0.0014	0.0014	0.0020	0.0008	0.0005	0.0005
B_v^{SEE}	0.0050	0.0056	0.0068	0.0082	0.0078	0.0071	0.0040	0.0032	0.0034
B_w^{SEE}	0.0051	0.0055	0.0056	0.0036	0.0066	0.0091	0.0060	0.0040	0.0031
B_u^{fit+}	0.0106	0.0106	0.0106	0.0106	0.0106	0.0106	0.0106	0.0106	0.0106
B_u^{fit-}	0.0470	0.0470	0.0470	0.0470	0.0470	0.0470	0.0470	0.0470	0.0470
B_v^{fit+}	0.0134	0.0134	0.0134	0.0134	0.0134	0.0134	0.0134	0.0134	0.0134
B_v^{fit-}	0.0058	0.0058	0.0058	0.0058	0.0058	0.0058	0.0058	0.0058	0.0058
B_w^{fit+}	0.0132	0.0132	0.0132	0.0132	0.0132	0.0132	0.0132	0.0132	0.0132
B_w^{fit-}	0.0087	0.0087	0.0087	0.0087	0.0087	0.0087	0.0087	0.0087	0.0087
B_u^+	0.0106	0.0106	0.0107	0.0107	0.0107	0.0108	0.0106	0.0106	0.0106
B_u^-	0.0470	0.0470	0.0470	0.0470	0.0470	0.0470	0.0470	0.0470	0.0470
B_v^+	0.0143	0.0145	0.0150	0.0157	0.0155	0.0151	0.0140	0.0138	0.0138
B_v^-	0.0077	0.0080	0.0089	0.0101	0.0097	0.0091	0.0070	0.0066	0.0067
B_w^+	0.0142	0.0143	0.0143	0.0137	0.0148	0.0160	0.0145	0.0138	0.0136
B_w^-	0.0101	0.0103	0.0103	0.0094	0.0109	0.0126	0.0106	0.0096	0.0092
S_u	0.0017	0.0020	0.0026	0.0040	0.0040	0.0033	0.0047	0.0049	0.0025
S_v	0.0007	0.0011	0.0018	0.0025	0.0025	0.0049	0.0029	0.0039	0.0015
S_w	0.0034	0.0029	0.0019	0.0039	0.0056	0.0034	0.0049	0.0032	0.0026
U_u^+	0.0112	0.0114	0.0118	0.0134	0.0133	0.0127	0.0142	0.0145	0.0118
U_u^-	0.0471	0.0472	0.0473	0.0477	0.0477	0.0475	0.0480	0.0480	0.0473
U_v^+	0.0144	0.0147	0.0155	0.0165	0.0163	0.0180	0.0151	0.0159	0.0141
U_v^-	0.0078	0.0084	0.0096	0.0112	0.0110	0.0134	0.0091	0.0103	0.0074
U_w^+	0.0157	0.0155	0.0148	0.0158	0.0185	0.0174	0.0175	0.0152	0.0146
U_w^-	0.0122	0.0118	0.0110	0.0123	0.0156	0.0143	0.0144	0.0115	0.0106
u	1.0266	1.0187	0.9648	0.8962	0.9411	0.9636	1.0660	1.1415	1.1566
v	-0.1734	-0.2088	-0.2528	-0.2782	-0.2830	-0.2370	-0.0972	-0.0246	0.0123
w	-0.2300	-0.2457	-0.2208	-0.0928	0.1589	0.3834	0.2038	0.0605	-0.0149

SRI M. S. No. 631

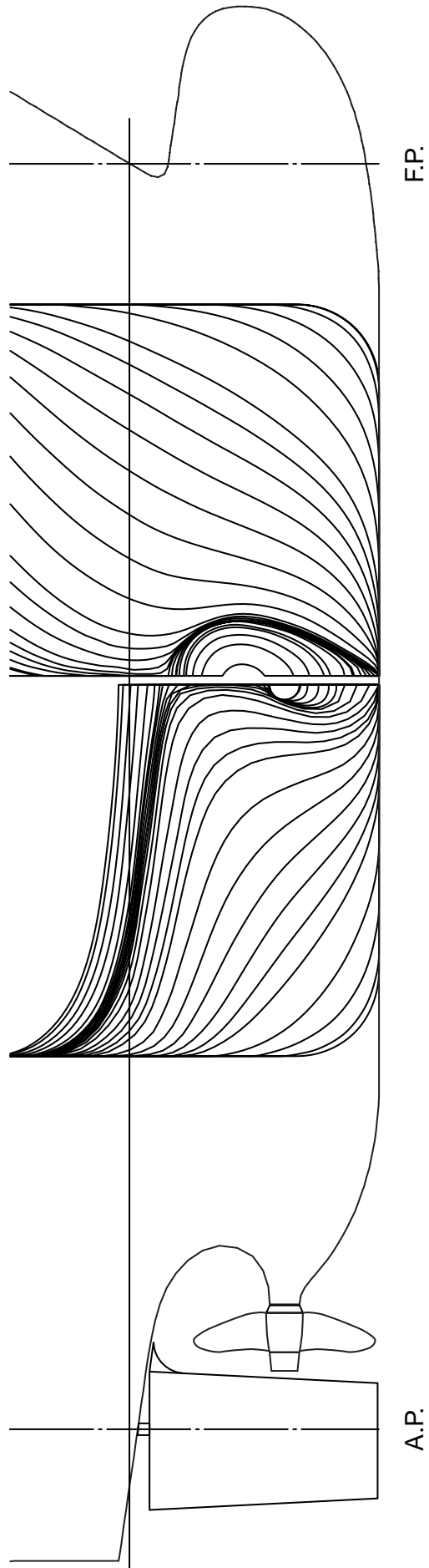


Fig. 1 Body Plan and Side Profile of Ship Model, SRI M. S. No. 631

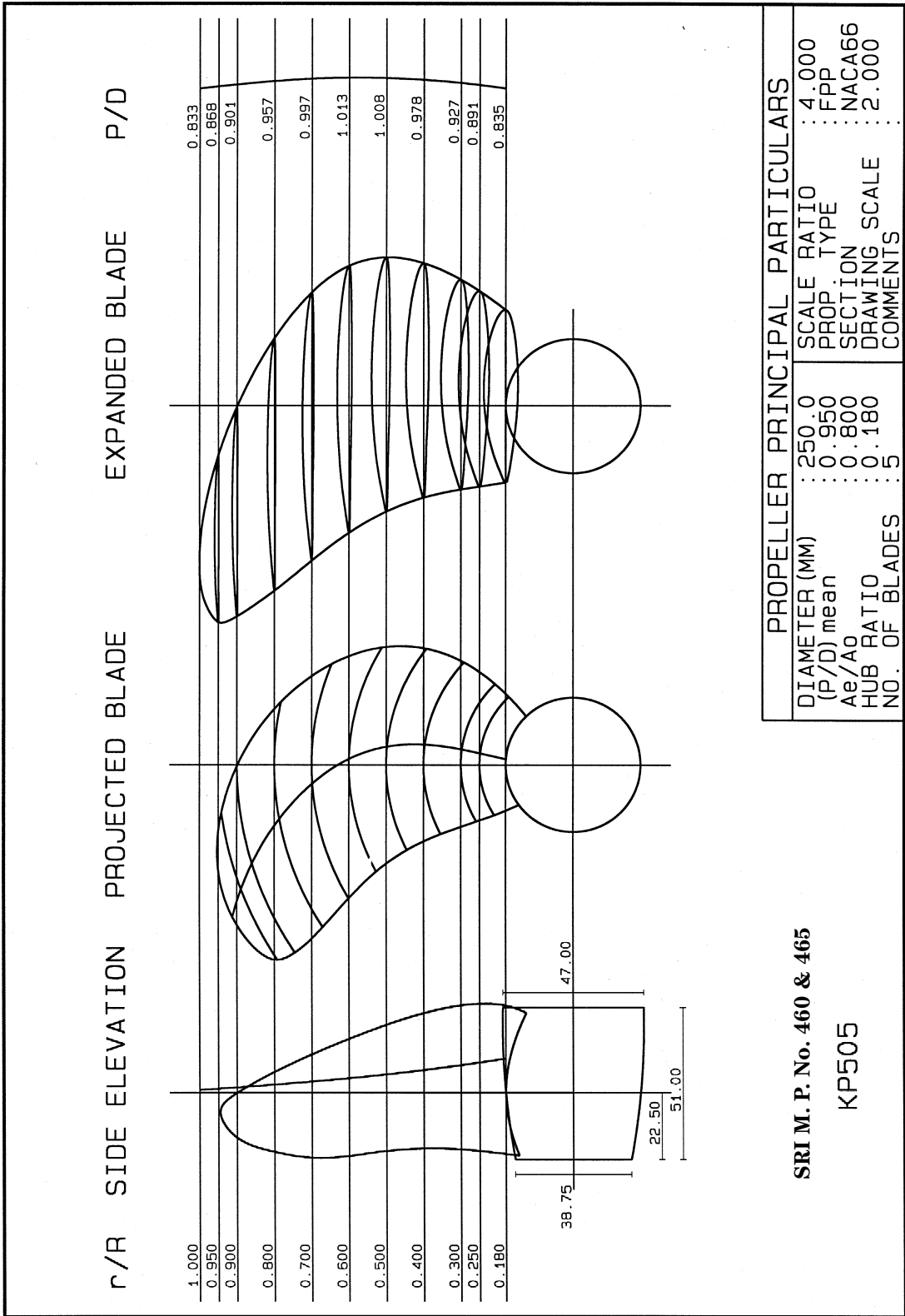


Fig. 2 Geometrical Shape Model of Propeller, SRI M. P. No. 460 & 465

8-Hole Pitot Tube

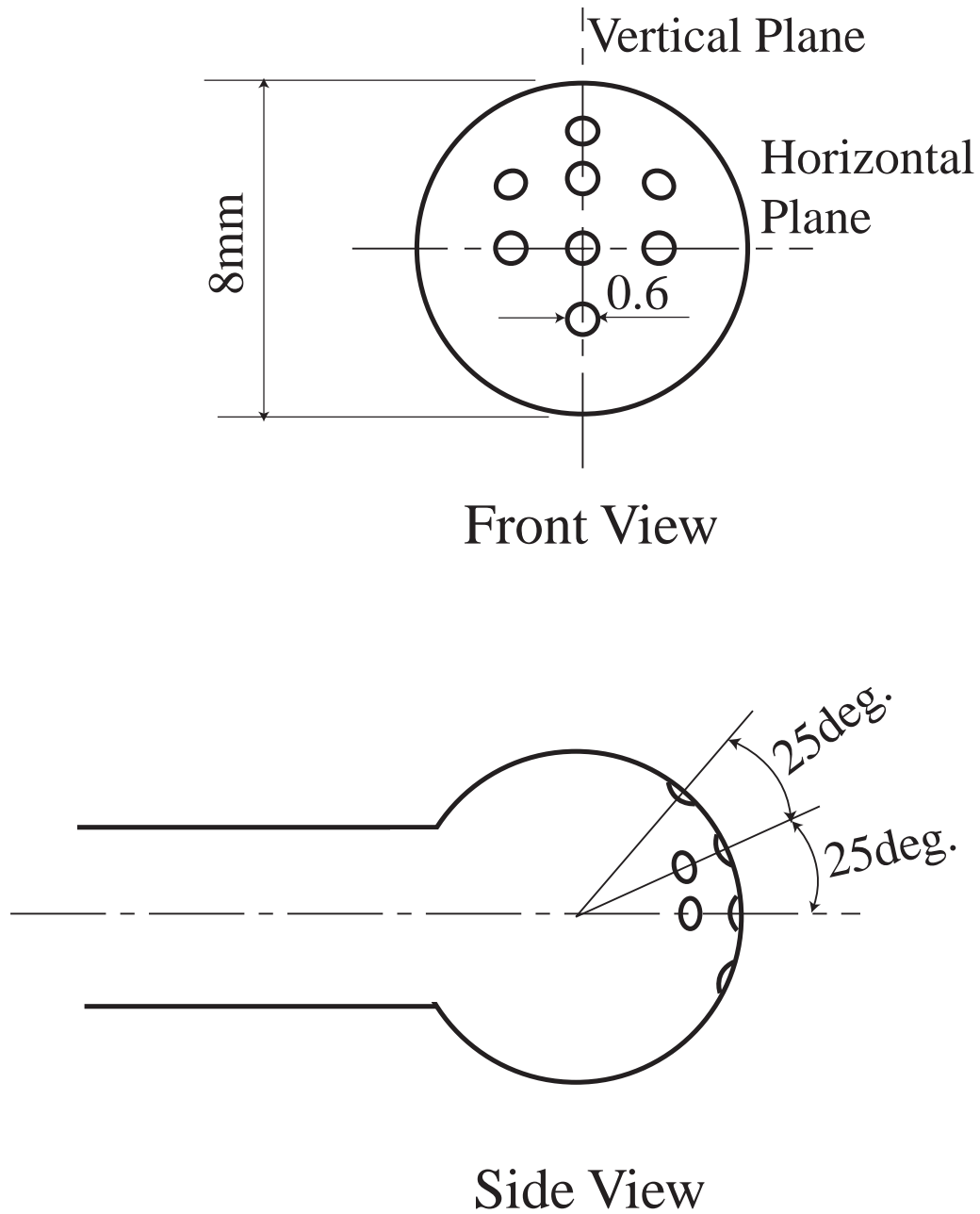


Fig. 3 Geometrical Shape of Eight-Hole Pitot Tube